FIREFIGHTING ROBOT WITH VIDEO FULL-CLOSED LOOP CONTROL

H.B. WU, Z.J. LI, J.H. YE, S.C. MA, J.W. LI & X.N. YANG
School of Mechanical Engineering and Automation, Fuzhou University, China.

ABSTRACT

In view of the many problems in firefighting robots, such as complicated flame positioning, poor environmental adaptability, and difficult installation and debugging, a new firefighting robot design is presented with video full closed-loop feedback to extinguish ground fire in this paper. The firefighting robot consists of a 2-DOF robot, a monocular camera, and a controller. The monocular camera installed on the second link of the robot is utilized to detect and locate ground flames. The robot can dynamically adjust the water landing point to track a flame in real-time through motion control, as the camera is specifically designed with an additional infrared narrowband pass filter and a filter-switching mechanism. An algorithm of detecting and positioning for flame and water landing point is proposed based on image processing and robotic kinematics. Experimental results show that the firefighting robot with video full closed-loop feedback can realize real-time flame detection, location, and sprinkler, and can dynamically track fire location within the monitoring scope. The distance error between fire and the landing point of the water jet can be controlled within a narrow range. Moreover, this firefighting robot is easy to install, debug and have good environment adaptability, and provides efficient and safe solutions for complicated firefighting environment. At the same time, due to its small size and convenient calibration features, this firefighting robot is especially suitable for large space environments.

Keywords: firefighting robot, flame location, full closed-loop control video detection, water landing point detection.

1 INTRODUCTION

Fire often causes enormous loss to human life and properties. Thus, to control and extinguish fire hazards, many types of firefighting equipment have emerged. In the current building fire protection design, fire detections, such as gas or smoke and temperature sensors [1], and fire extinguishing methods, such as automatic sprinkler systems, are commonly adopted [2, 3]. Video-based technology or computer vision methods are also used in some firefighting system [4]. However, these kinds of fire detections and fire extinguishing equipment are not automatically linked to one another or work cooperatively. The traditional fire extinguishing system can also not effectively spray water at any place and may lead to unnecessary loss of too much water [5, 6]. To cope with this problem, automatic firefighting robots are invented for automatic fire detection and sprinkling, which already have certain domestic and foreign research and applications in recent years [7, 8]. Automatic firefighting robots usually adopt pyroelectric infrared flame detection technology. Sensors installed on the firefighting robot with the moving robot to search and locate a fire source [9, 10]. However, this fire detection method is easily affected by the vibration of robotic motion, external temperature change and electromagnetic interference, which may cause false alarms and omission alarms. In addition, infrared sensors cannot completely identify the fire shape and size, and this may cause water landing point deviated from the center of the fire and fire extinguishing efficiency reduced [11, 12]. Therefore, some researchers are trying to use multi-sensor fusion techniques and intelligent algorithm to improve performance of the system [13–15], but it makes the system too complex and unpractical.

ISSN: 2041-9031 (paper format), ISSN: 2041-904X (online), http://www.witpress.com/journals
DOI: 10.2495/SAFE-V6-N2-254-269

Video detection combining image-processing technology is an effective method in firefighting system, and some work has been done by researchers [2, 16, 17]. Rossi, Verstockt, and Hsu proposed a video fire detection technology with a huge amount of information for automatic firefighting robots [18–20]. Based on binocular stereo vision technology in fire detection and positioning has attracted much attention recently. Li, Lu and Yan proposed a stereoscopic imaging technique by A low-cost binocular CCD camera for fire detection [21]. Utilizing two or more cameras to form stereo vision can achieve a 3D reconstruction of a fire and locate a fire accurately [22, 23]. A kind of 3D location method based on sub-pixel edge detection and non-parametric stereo matching technology was explored to cope with imprecise camera calibration and unstable stereo matching [24]. However, the calibrations for cameras of binocular stereo vision system need to take many distortion factors into consideration. This calibration process is complicated and specialized. The robot link yet normally has no such space to install the multiple camera stereo vision system. The coordinate systems require reestablishment and recalculation for different applications. The algorithm to extract the fire source position is sophisticated and time-consuming [25]. Foggia proposed a real-time fire detection method that is able to detect fires by analyzing videos acquired by surveillance cameras [26]. But this method is based on a multi-expert system and limited its application. Therefore, the use of such multiple camera fire detection system is inconvenient for poor environmental adaptability, complex fire localization, difficult installation and debugging. Configuration of multiple cameras also considerably increases the system cost.

In the process of fire fighting, only getting fire location cannot ensure accurate fire extinguishing for firefighting robot, because water jet trajectory spewing from the robot may be deviated under the influence of robot manufacture errors, installation errors, and water pressure fluctuation [20]. In this study, a firefighting robot design was proposed based on video full closed-loop feedback with a monocular camera. The proposed design scheme can make water jet track ground fire source dynamically for precise positioning and fire extinguishing.

The paper is organized as follows: section II presents the overall scheme of firefighting robot based on video full closed-loop feedback. Section III discusses location algorithm of the fire image. Section IV describes image recognition of the water jet. Section V shows the experimental setup and results with the proposed algorithm. Finally, it is summarized in section VI.

2 OVERALL SCHEME OF FIREFIGHTING ROBOT BASED ON VIDEO FULL CLOSED-LOOP FEEDBACK

The firefighting robot based on video full closed-loop feedback consists of a robot body, a camera and a robot controller, as shown in Fig. 1.

The robot body consists of two joints. The first joint can make the robot rotate around a vertical axis in the horizontal plane, and the second joint can make the robot forearm rotate around a horizontal axis in the vertical plane. A camera installed on robot link 2 can monitor different directions while joint 1 is rotating, and can achieve a full 360-degree scan. In addition, the pitch angle of the camera can be changed while joint 2 is rotating to adjust the camera monitoring scope. Given a hollow design of the robot link interior, firefighting water can be imported externally into the robot base and then sprayed from the end of the robot through a hollow pipeline. Thus, by controlling the movement of the robot, the detection and localization of fire as well as the sprinkler can be realized. The controller consists of an industrial control computer and robot joint drive components. The computer can quickly process camera video signals and send instructions to control the movement of the robot via the joint drive components.

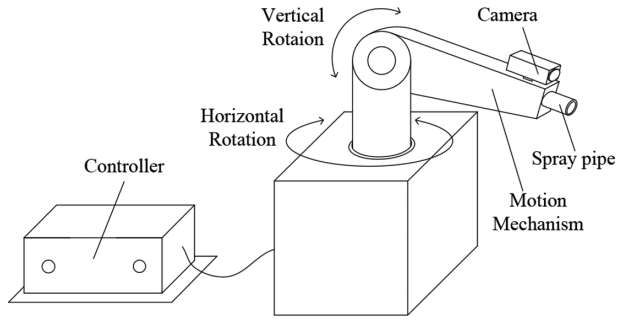

Figure 1: Design scheme of a firefighting robot based on video full closed-loop feedback.

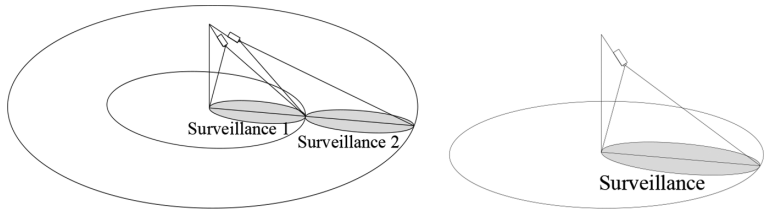

(a) Double scanning (b) Single scanning

Figure 2: Detection methods of different monitoring areas.

The visual inspection area of the camera on the ground can be changed by controlling the movement of the robot. If the monitoring radius is too large that the camera perspective projection becomes insufficient to cover the entire radius area, the monitoring area can be divided into two regions. Particularly, the robot rotates horizontally to scan the inner ring first, and then the robot scans the outer ring by adjusting the vertical elevation angle, as shown in Fig. 2a. Otherwise, the robot rotates horizontally to scan the entire monitoring area, as shown in Fig. 2b.

Monocular vision method is adopted in this paper. The camera is utilized to realize two functions: to detect and locate a fire and the water jet landing point. When fire occurs in the protected area, the controller is activated by the external fire signal, and then the controller controls the robot to scan the protected area 360° horizontally while collecting and processing image information obtained from the camera in real time. Once the fire image information is confirmed, the robot stops scanning and calculates the actual position of the fire on the ground. Subsequently, the controller drives joints 1 and 2 rotation and direct the water jet toward the fire source. During fire extinguishing, the controller detects the water landing point and the fire source position in real time and dynamically adjusts the water landing point to track the coordinates of the fire. Consequently, through the video full-closed loop feedback control, the firefighting robot can extinguish fire accurately and efficiently.

Adopting a conventional colored camera to detect fire, disturbances such as sunlight reflection, lighting, and ground light often cause false fire detection, and affect the practical application. A burning fire always releases large amounts of CO_2. The spectral analysis of a

(a) Original image (b) Image with a filter

Figure 3: Comparison of the image with and without an optical filter.

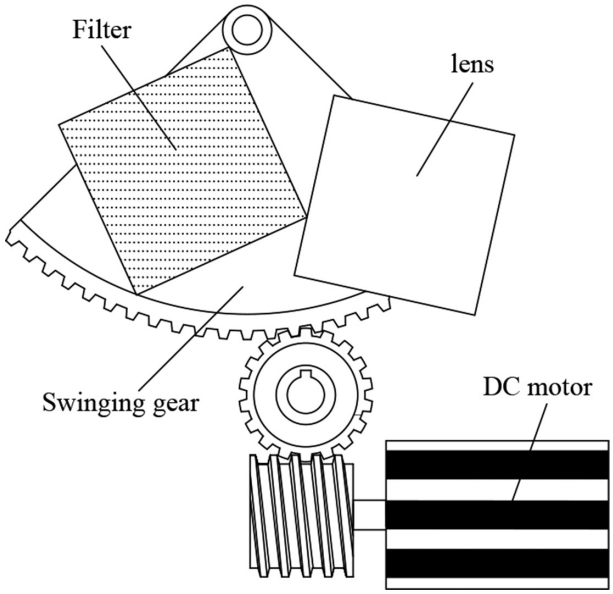

Figure 4: Principle of the filter-switching device.

burning fire shows that an obvious radiation peak appears around the 4.2 μm infrared band, which is a specific characteristic of fire [27]. Therefore, this firefighting robot adds a 4.2–4.5 μm narrow bandpass optical filter in the front end of the camera charge-coupled device (CCD) sensor. The optical filter can effectively eliminate various optical interferences while retaining the fire characteristic of the infrared. Figure 3a shows a fire image collected during a sunny summer noontime without a filter. Figure 3b shows a fire image obtained after adding a filter. According to the comparison between Fig. 3a and 3b, the roadside vehicles, trees, and persons wearing white shirts, which reflect light excellently, all present weak brightness after the filter is added. In addition, in spite of the sunshine on the ground, a high-brightness characteristic of the fire is still evident in the image. This finding shows that adding a filter can strip the background well and help to extract useful information of the fire.

Adding an optical filter can significantly improve fire detection. However, adding a filter is not conducive to detect water jet and water landing points, which should both be detected under a natural light background. Therefore, a specialized filter-switching device is introduced

in the internal design of the camera. This device consists of different parts such as a small DC motor and gear mechanism, as shown in Fig. 4.

3 LOCATION ALGORITHM OF THE FIRE IMAGE

To realize ground fire location, a coordinate system must be established first. As shown in Fig. 5, *XYZ* is the geodetic coordinate system, and *O* is the origin point of *XYZ*. The firefighting robot is rightly above *O*. $X_1Y_1Z_1$ is the robot base coordinate system, and *H* is the installation height which can be measured in site and input into the system. A camera is installed on the second link of the robot, and the optical axis is parallel to the water jet outlet direction. $X_2Y_2Z_2$ is the camera coordinate system, and $(X_0,Y_0,0)$ is the point of the fire in the geodetic coordinate system.

The camera elevation angle can be adjusted according to the installation height *H* of the robot, detection range, and camera lens parameters for the camera view to cover the entire monitoring area of the radius direction. When a fire occurs in the monitoring area, the robot stops moving horizontally once the fire source in the image is detected. Here, the horizontal and vertical rotation angles of the robot are θ_{10} and θ_{20}, respectively.

The camera image coordinate system is shown as Fig. 6a, where *f* is the camera focal distance, A(*X*,*Y*,*Z*) is the coordinate of the fire source bottom center in the camera coordinate

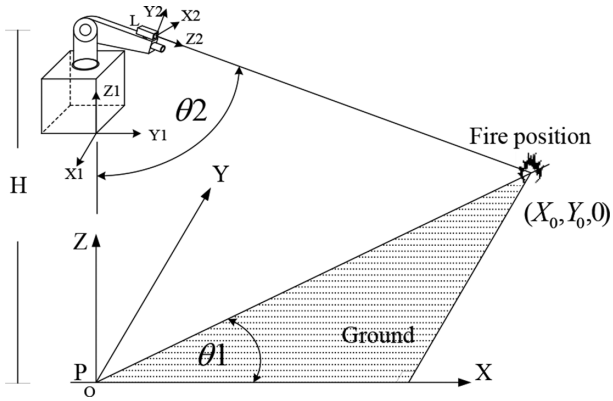

Figure 5: Fire detection model of the firefighting robot.

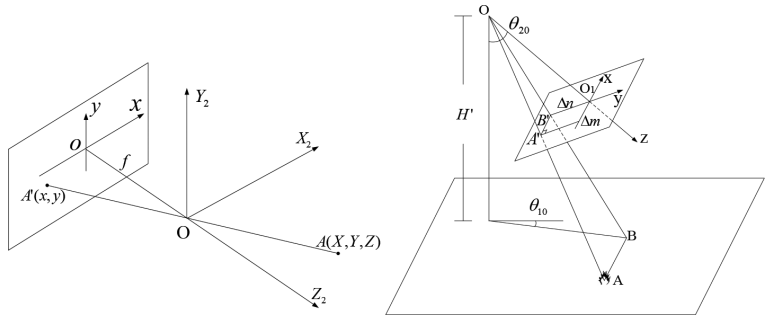

Figure 6: Principle of fire location. (a) Image coordinate system on the visual plane xy (b) Image coordinate system in the space.

system $X_2Y_2Z_2$, and $A'(x, y)$ is the projection coordinate of A(X,Y,Z) on the visual plane xy. The relationship between $A'(x, y)$ and A(X,Y,Z) is as follows:

$$x = f\frac{X}{Z}, y = f\frac{Y}{Z}. \tag{1}$$

According to the above mathematical model, the ground coordinate of the fire source can be introduced.

The coordinate of the fire source in the ground coordinate system can be achieved through coordinate transformation from the camera coordinate to the ground coordinate. This calculation can be simplified according to monocular visual imaging characteristics [28]. The image coordinate system is located in the ground coordinate, as shown in Fig. 6b, where O is the camera focal point, O_1 is the center point of the visual plane, A is the center point of the fire bottom, A' is the projection point of A on the visual plane, and AB is the intersecting line between plane $OA'B'$ and the ground plane. Δm and Δn are the horizontal and vertical distances from point A' to the center of the visual plane, respectively. The image pixel is converted into the actual length first to calculate the actual distance. In the visual plane, assuming that P is the linear image resolution (ppi) and the actual length of each pixel is 0.0254/P (meter), the actual offset length between the image center and the fire center can be calculated as follows:

$$(\Delta m, \Delta n) = 0.0254 \times (x, y) / P. \tag{2}$$

Given that the camera is installed on the second link of the robot, the image coordinate system moves up and down with the second link. Thus, the distance H' of the focus point to the ground varies. H' can be calculated as:

$$H' = H - L\cos\theta_{20}, \tag{3}$$

where L is the length of the second link.

According to the position relationship of the two triangles OAB and $OA'B'$ in Fig. 6b, the X coordinate of the fire source point in the camera coordinate system $X_2Y_2Z_2$ can be expressed as:

$$X = -\frac{\Delta m H'}{\cos(\theta_{20} - \arctan\frac{\Delta n}{f})\sqrt{f^2 + \Delta n^2}}. \tag{4}$$

Furthermore, the y and z coordinates of the fire source point in the camera coordinate system can be calculated as follows:

$$Y = X\Delta n / \Delta m, Z = fX / \Delta m. \tag{5}$$

According to the principle of robotic kinematics and coordinate transformation, the coordinate system of robot links is established as shown in Fig. 7.

The camera coordinate system can be converted into a geodetic coordinate system through the following transformation matrix:

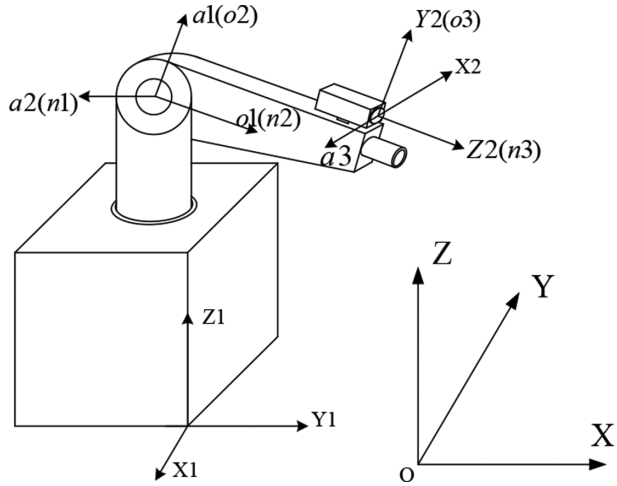

Figure 7: Robotic coordinate transformation.

$$A_0 = \begin{bmatrix} \cos(-90°) & -\sin(-90°) & 0 & H\cos(-90°) \\ \sin(-90°) & \cos(-90°) & 0 & H\sin(-90°) \\ 0 & 0 & 1 & 0 \\ 0 & 0 & 0 & 1 \end{bmatrix}, \quad A_1 = \begin{bmatrix} \cos\theta_{10} & 0 & \sin\theta_{10} & 0 \\ \sin\theta_{10} & 0 & -\cos\theta_{10} & 0 \\ 0 & 1 & 0 & 0 \\ 0 & 0 & 0 & 1 \end{bmatrix},$$

$$A_2 = \begin{bmatrix} \cos\theta_{20} & -\sin\theta_{20} & 0 & L\cos\theta_{20} \\ \sin\theta_{20} & \cos\theta_{20} & 0 & L\sin\theta_{20} \\ 0 & 0 & 1 & 0 \\ 0 & 0 & 0 & 1 \end{bmatrix}, \quad A_3 = \begin{bmatrix} 0 & 0 & 1 & 0 \\ 0 & 1 & 0 & 0 \\ -1 & 0 & 0 & 0 \\ 0 & 0 & 0 & 1 \end{bmatrix},$$

$$A = A_0 A_1 A_2 A_3 = \begin{bmatrix} \cos\theta_{10} & -\sin\theta_{10}\sin\theta_{20} & \sin\theta_{10}\cos\theta_{20} & L\sin\theta_{10}\cos\theta_{20} \\ \sin\theta_{10} & \cos\theta_{10}\sin\theta_{20} & -\cos\theta_{10}\cos\theta_{20} & -L\cos\theta_{10}\cos\theta_{20} - H \\ 0 & \cos\theta_{20} & \sin\theta_{20} & L\sin\theta_{20} \\ 0 & 0 & 0 & 1 \end{bmatrix} \quad (6)$$

where A_0, A_1, A_2, and A_3 are the transformation matrices from the coordinate systems XYZ, $n_1o_1a_1$, $n_2o_2a_2$, and $n_3o_3a_3$ to the coordinate systems $n_1o_1a_1$, $n_2o_2a_2$, $n_3o_3a_3$ and $X_2Y_2Z_2$, respectively.

Z_0 is 0 for the ground fire, thus, the geodetic coordinate of the ground fire can be obtained as:

$$\begin{bmatrix} X_{fire} \\ Y_{fire} \\ 0 \\ 1 \end{bmatrix} = A \begin{bmatrix} X \\ Y \\ Z \\ 1 \end{bmatrix} = \begin{bmatrix} \cos\theta_{10}X - \sin\theta_{10}\sin\theta_{20}Y + \sin\theta_{10}\cos\theta_{20}Z + L\sin\theta_{10}\cos\theta_{20} \\ \sin\theta_{10}X + \cos\theta_{10}\sin\theta_{20}Y - \cos\theta_{10}\cos\theta_{20}Z - L\cos\theta_{10}\cos\theta_{20} - H \\ 0 \\ 1 \end{bmatrix}. \quad (7)$$

Furthermore, when the water jet is orientated to the fire source, the horizontal angle θ_1 of the first joint and the vertical angle θ_2 of the second joint can be expressed, respectively, as follows:

$$\theta_1 = \arctan(Y_{fire} / X_{fire}), \theta_2 = \arctan(\sqrt{X_0^2 + Y_0^2} / H). \tag{8}$$

However, using this set of angle parameters to control the firefighting robot cannot solve the firefighting problem. Notably, given that the water jet trajectory is parabolic, a certain deviation still exists between the water landing point and the fire source point even when the water outlet of the robot is directly orientated to the fire source. For instance, when the water initial velocity is a constant, the water jet cannot be loading in the fire location due to the water gravity and air resistance. Therefore, the elevation angle of the robot outlet should be compensated before spraying water. Consider in the aspects of firefighting system itself, the compensation $\Delta\theta$ is related to the factors of water initial velocity, elevation angle, and water jet height. Given that the water jet is greatly influenced by various external factors, but no proper theoretical algorithm can accurately describe the water jet trajectory at present. Nevertheless, some relationship can be drawn by theoretical analysis and experiment. When the camera installation height and water spraying pressure are constant, $\Delta\theta$ is mainly determined by the elevation angle of the robot water outlet. Thus, through numerous water spraying experiments, we obtain the following experience calculation method:

$$\Delta\theta = \begin{cases} 0 & if(\theta_2 < 35°) \\ k_1(\theta_2 - 35°) & if(35° \le \theta_2 < 50°) \\ k_2(\theta_2 - 50°) & if(50° \le \theta_2 < 55°) \\ k_3(\theta_2 - 55°) & if(55° \le \theta_2 < 60°) \\ k_4(\theta_2 - 60°) & if(60° \le \theta_2 < 65°) \end{cases}, \tag{9}$$

where the parameters k_1, k_2, k_3, k_4 require calibration according to the camera installation height and water spraying pressure. In most cases, when θ_2 exceeds 65°, identifying a little fire on the ground that is far from the robot becomes very difficult for the camera. Therefore, the angle range of θ_2 is set to 0°–65°.

During firefighting, the robot rotates on the first joint while detecting fire on the ground. Once a fire is detected, the robot rotates only on the first joint for θ_1 horizontally, while rotating at the second joint for $\theta_2 + \Delta\theta$ vertically, and then extinguishing fire directly.

4 IMAGE RECOGNITION OF THE WATER JET

After fire location and elevation angle compensation, the water jet may still not fall on the fire center because of the factors such as robot structural error, camera installation error, water pressure variation and wind velocity [29]. The robot then requires further dynamic adjustment according to the deviation between the water landing point and the fire source center. In addition, the robot is required to identify the water jet trajectory and water landing point.

To extract the water landing point, the water flow trajectory should be primarily extracted from the image frames of the colored video. The gray feature of the water flow trajectory is obvious, as shown in Fig. 8. Figure 8b shows the result of Fig. 8a after binary image processing and filtering of the impurity points. As shown in Fig. 8b, other disturbed areas, such as numbers 1 and 2, may exist aside from the water jet area number 3. These disturbed areas

(a) Original image (b) After gray binarization

Figure 8: Image graying of the water jet.

may be the burning fire or sump under the sunlight. Rejecting the disturbance is normally easy because the water jet is characterized with obvious directivity streamline and large area. The water jet area is an image with thin consistency and occupies a large proportion of the total image.

To obtain the position of the water landing point, the starting point of the water jet area in an image should be extracted first, and then the entire water jet trajectory is extracted until the coordinate of the water landing point is determined ultimately. Thus, after binary image processing, impurity points filtering and interference elimination of the original image which captured from the camera, the entire water jet can be obtained. Through numerous field experiments and optimization, the calculation formula of the gray value D can be expressed as follows:

$$D = 0.114 \times B + 0.587 \times G + 0.299 \times R, \tag{10}$$

where R, G, and B represent the image pixel values of the red, green, and blue (RGB) channels, respectively.

By analyzing a large number of water jet trajectory images, we can conclude that besides the obvious grayscale characteristics, the color characteristics of all the points in the water jet trajectory are similar. In an RGB color space, the sum of the absolute values of the color difference between two adjacent points is minimal. The adjacent points with the minimum chromatic aberration in the RGB space should be in the water jet trajectory [30]. The chromatic aberration between two points can be calculated as follows:

$$C_{(M-N)} = |R_M - R_N| + |G_M - G_N| + |B_M - B_N|. \tag{11}$$

The principle of water jet trajectory pixel scanning is shown in Fig. 9. From the first line pixels to the last line pixels in the image, some pixels with larger gray values, such as $X_{(i,b-5)}$,$X_{(i,b-4)}$…$X_{(i,b+4)}$,$X_{(i,b+5)}$ are extracted, and then a point near the middle of these values with a maximum gray value is selected in every line pixel, as shown by Mi in Fig. 9.

When the water jet reaches the ground, water is dispersed toward all directions. Not all of the above-dispersed points are on the water jet trajectory. The point of intersection between the water jet trajectory and the ground is the water landing point. When the water jet reaches the ground, the color, and gray characteristics of the water jet change greatly, and these characteristics can be utilized to determine the water landing point. The formula for this scenario can be defined as:

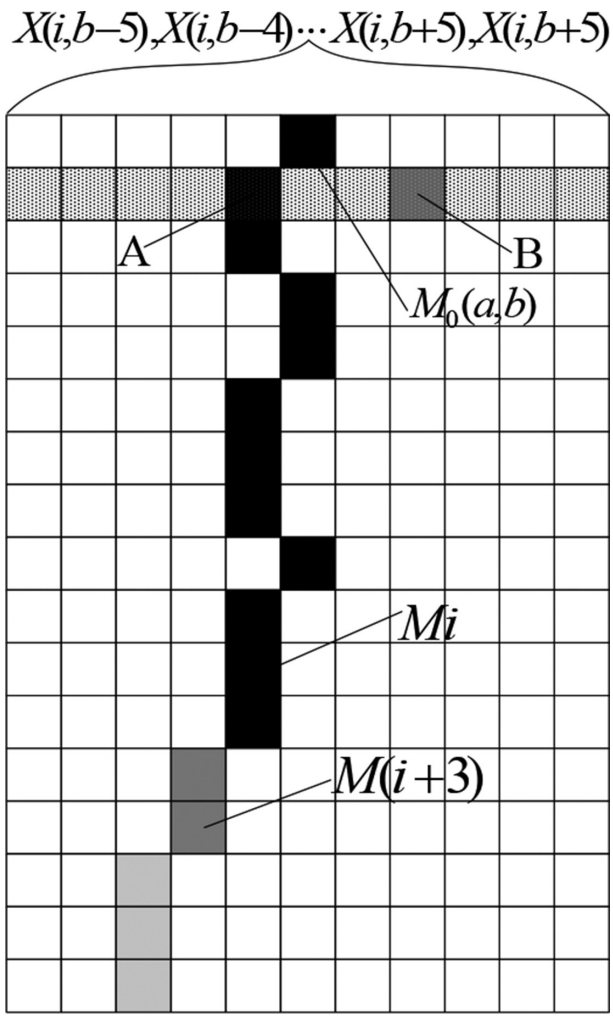

Figure 9: Pixel scanning image of the water jet trajectory.

$$T_1 = | D_{M(i+3)} - D_{Mi} | + C_{(M(i+3)-Mi)}, \tag{12}$$

where $i = 0, 1, 2 \ldots\ldots n$; D_{Mi} and $D_{M(i+3)}$ are the gray values of marking points M_i and $M_{(i+3)}$, respectively, and $C_{(M(i+3)-Mi)}$ is the value of the chromatic aberration between M_i and $M_{(i+3)}$.

The T_d presented in this paper is a threshold. The controller then scans all the pixels from the first line. For the pixels of each line, $T_1 < T_d$ denotes that the water jet is not terminated, as shown by the red mark in Fig. 10; otherwise, the water jet is terminated, which is regarded as the water landing point.

The water landing point can be regarded as the intersection point between the water jet trajectory and the ground. To obtain the coordinate of the water landing point, the water jet trajectory line should be fitted first. The water jet trajectory is linear in the image because the camera and the water outlet are on the same vertical plane. According to the linear equation,

Figure 10: Water landing point extraction.

$y = a_0 + a_1 x$ and the least squares method, the water jet trajectory is fitted, as shown in Fig. 10. Parameters a_0 and a_1 can be calculated through the fitting matrix equation:

$$\begin{bmatrix} n & \sum X_{M_i} \\ \sum X_{M_i} & \sum X_{M_i}^2 \end{bmatrix} \begin{bmatrix} a_0 \\ a_1 \end{bmatrix} = \begin{bmatrix} \sum Y_{Mi} \\ \sum X_{M_i} Y_{Mi} \end{bmatrix}. \tag{13}$$

The coordinate of the water landing point satisfies the following formula:

$$\min \left| Y_{Mi} - a_0 - a_1 X_{Mi} \right|. \tag{14}$$

5 EXPERIMENT

A firefighting robot was developed to verify the firefighting robot design based on video full closed-loop feedback, as shown in Fig. 11. A camera was installed in the front end of the spray pipe. The robot can then rotate horizontally and vertically together with the camera.

When the firefighting robot is working, the camera will always be real-time image acquisition. The fire images captured by the camera are shown in Fig. 12a (with optical filter installed). After implementing the algorithms, such as the graying algorithm and expansion corrosion algorithm [31, 32], the processed image as shown in Fig. 12b. From comparison of two figures, the fire information can be evidently extracted completely after processing. The pixel coordinate of the fire center in the image can also be obtained. If the fire is larger, it's more easier to be identified and find the fire center.

In the experiments, during the day, the firefighting robot was installed on a platform mounted on a 25-meter high building roof. A movable fire source for the test can be located anywhere within the scope of the 60-meter ground radius. During the tests, the fire source was located in five coordinate points of (15, 15), (25, 25), (35, 35) and (45, 45) (the unit is meter) to perform the firefighting experiments. The water flow was scattered from the water outlet of the robot. Thus, the water landing point was not an actual point but a relatively large circle. If the scattered water circle covers the fire source, the fire will be extinguished, and this circle will be expanded with the spraying distance increasing. In every test, the fire source was a fire pan with a diameter of 0.5 meter and the fuel used was 1.0-liter gasoline. Some

Figure 11: Firefighting robot.

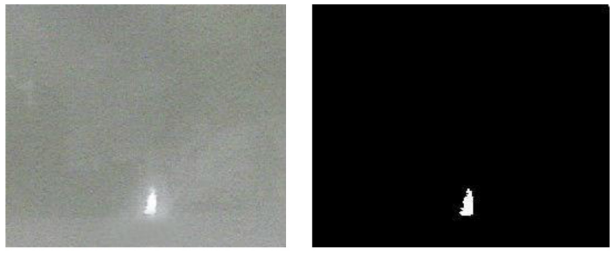

(a) Original image (b) Image after processing

Figure 12: Fire image process.

experimental data were obtained, as shown in Fig. 13. Evidently, the coordinate error increased as the distance increased. Within the 60-meter monitoring scope, the localization error in distance between the fire source center and the water landing center can be limited in an allowable value of about 1 to 2 meter and the fire source can be extinguished within a specified 3 min according to CECS245:2009.

Notably, if the elevation angle after compensation was too large, causing the fire source and the water jet to exceed the camera view, the robot cannot realize the closed-loop control. Figure 14 shows four frames of the video during the firefighting. The direction and elevation

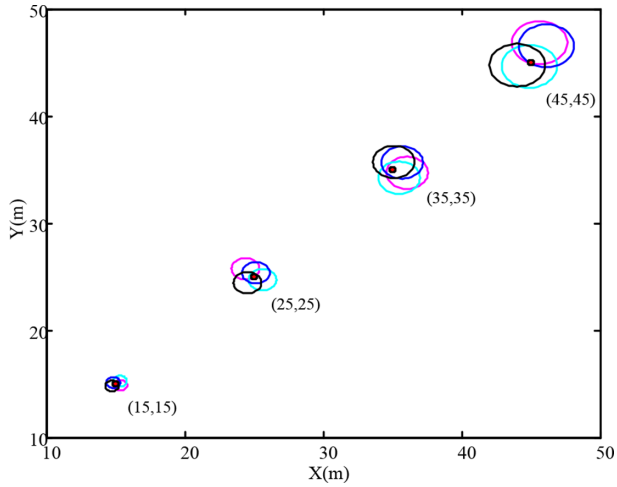

Figure 13: Experimental data of the fire localization algorithm.

(a)Fire tracking(1 min 41.5 s) (b)Fire tracking(1 min 43.5 s)

(c)Fire tracking (1 min 46.5 s) (d) Fire tracking (1 min 50 s)

Figure 14: Video screenshot of the water landing point tracking the fire.

angle of the water outlet can be dynamically adjusted according to the error between water landing coordinate and fire coordinate at different moments to realize the water landing point tracking the fire target. The fire source has to be placed in a narrow fan-shaped region in the tests because of the buildings around the experiment field. Approximately, 50 tests were performed to verify the firefighting effect. The average fire extinguishing time was 1 min 53 s. A total of 3 tests failed because the fire pan was overturned by water jet impacting.

6 CONCLUSION

We proposed a firefighting robot with video full-closed control to satisfy the requirement for modern fire protection. The robot was installed with an appropriative camera with special design moving to detect a fire. The image was processed using a controller to obtain the ground coordinates of the fire. The required joint angular displacement was calculated by the controller to control the robot to extinguish the fire based on robotic kinematics equation and elevation angle compensation algorithm. The experimental results showed that the location errors of the fire source and the water landing point were acceptable. During the water spraying process, the water landing point and the fire position coordinates were detected in real time, which were utilized to adjust the water landing point dynamically. Given that the detection of the water jet trajectory and the water landing point required a certain brightness of ambient light, the firefighting robot can achieve excellent fire extinguishing effect and efficiency during daytime. However, the robot has greater uncertainty at night because it relies on the lighting of the fire in the absence of a favorable ambient light. The case of firefighting in night needs to be further studied. In addition, the fire to be extinguished by the proposed firefighting robot was limited on the ground. If a fire ignited on wall or ceiling, the proposed firefighting robot cannot locate and extinguish the fire accurately since monocular vision configuration.

ACKNOWLEDGMENTS

This study is supported by the National Natural Science Foundation of China (No. 51175084 and 51575111), and University-Enterprise Cooperation Project (2015H6012).

REFERENCES

[1] Bogue, R., Sensors for fire detection. *Sensor Review*, **33**(2), pp. 99–103, 2013. http://dx.doi.org/10.1108/02602281311299635

[2] Liu, Z.G. & Kim, A.K., Review of recent developments in fire detection technologies. *Journal of Fire Protection Engineering*, **13**(2), pp. 129–151, 2003. http://dx.doi.org/10.1177/1042391503013002003

[3] Ding, H.J., Fan, D. & Yao, H.W., Cable tunnel fire experiments based on linear temperature sensing fire detectors. *Optics and Precision Engineering*, **21**(9), pp. 2225–2230, 2013. http://dx.doi.org/10.3788/OPE.20132109.2225

[4] Çetin, A.E., Dimitropoulos, K., Gouverneur, B., Grammalidis, N., Günay, O., Habiboglu, Y.H., Töreyin, B.U. & Verstockt, S., Video fire detection–review. *Digital Signal Processing*, **23**(6), pp. 1827–1843, 2013. http://dx.doi.org/10.1016/j.dsp.2013.07.003

[5] Rehman, A., Masood, N., Arif, S., Shahbaz, U., Sarwar, F., Maqsood, K. & Pasha, M., Autonomous fire extinguishing system. *Proceeding of International Conference on Robotics and Artificial Intelligence*, IEEE Computer Society, Washington, pp. 218–222, 2012. http://dx.doi.org/10.1109/icrai.2012.6413387

[6] Ahmed, H., Mohanad, E., Nour, J. & Mohammed, E., An autonomous firefighting robot. *Proceeding of the 17th International Conferences on Advanced Robotics*, IEEE Robotics and Automation Society, Turkey, pp. 530–535, 2015.

[7] Hu, G.L. & Li, Z., Design and key technology research into autotargeting fire extinguishing system of interior large space. *Proceeding of International Conferences on*

Electrical and Control Engineering, IEEE Computer Society, Piscataway, pp. 687–690, 2010.

[8] Yang, Q.M. & Sun, J.M., Design of an integrated location system for fire detecting robot. *Proceeding of 4th International Conferences on Fuzzy Systems and Knowledge Discovery*, Institute of Electrical and Electronics Engineers Inc., Piscataway, 3, pp. 327–330, 2007.
http://dx.doi.org/10.1109/fskd.2007.243

[9] Pack, D.J., Robert, A., Ahigren, D.J. & Verner, I.M., Fire fighting mobile robotics and interdisciplinary design-comparative perspectives. *IEEE Transactions on Education*, **47**(3), pp. 369–376, 2004.
http://dx.doi.org/10.1109/TE.2004.825547

[10] Khoon, T.N., Sebastian, P. & Saman, A.B.S., Autonomous fire fighting mobile platform. *Procedia Engineering*, **41**, pp. 1145–1153, 2012.
http://dx.doi.org/10.1016/j.proeng.2012.07.294

[11] Wang, X.G., Lo, S. & Zhang, H., Exploring the role of feature subset combinations on performance of multisensor fire detection. *Journal of Applied Fire Science*, **23**(2), pp. 179–192, 2013.
http://dx.doi.org/10.2190/AF.23.2.e

[12] Pesatori, A. & Norgia, M., Infrared image system for fire location. *Measuremen*t, **46**(10), pp. 4172–4178, 2013.
http://dx.doi.org/10.1016/j.measurement.2013.07.040

[13] Wang, S.D., He, Y.P., Zou, J.J, Duan, B.B. & Wang, J., A flame detection synthesis algorithm. *Fire Technology*, **50**(4), pp. 959–975, 2014.
http://dx.doi.org/10.1007/s10694-012-0321-6

[14] Mahdipour, E. & Dadkhah, C., Automatic fire detection based on soft computing techniques review from 2000 to 2010. *Artificial Intelligence Review*, **42**(4), pp. 895–934, 2014.
http://dx.doi.org/10.1007/s10462-012-9345-z

[15] Kim, J.H., Joseph, S. & Brian, L., Firefighting robot stereo infrared vision and radar sensor fusion for imaging through smoke. *Fire Technology*, **51**(4), pp. 823–845, 2015.
http://dx.doi.org/10.1007/s10694-014-0413-6

[16] Zhang, Z.J., Shen, T. & Zou, J.H., An improved probabilistic approach for fire detection in videos. *Fire Technology*, **50**(3), pp. 745–752, 2014.
http://dx.doi.org/10.1007/s10694-012-0253-1

[17] Zhang, H.J., Zhang, N. & Xiao, N.F., Fire detection and identification method based on visual attention mechanism. *Optik-International Journal for Light and Electron Optics*, **126**(24), pp. 5011–5018, 2015.
http://dx.doi.org/10.1016/j.ijleo.2015.09.167

[18] Rossi, L., Akhloufi, M. & Tison, Y., On the use of stereovision to develop a novel instrumentation system to extract geometric fire fronts characteristics. *Fire Safety Journal*, **46**(1), pp. 9–20, 2011.
http://dx.doi.org/10.1016/j.firesaf.2010.03.001

[19] Verstockt, S., Van Hoecke, S., Tilley, N., Merci, B., Sette, B., Lambert, P., Hollemeersch, C.F.J. & Van De Walle, R., Firecube: a multi-view localization framework for 3D fire analysis. *Fire Safety Journal*, **46**(5), pp. 262–275, 2011.
http://dx.doi.org/10.1016/j.firesaf.2011.03.001

[20] Hsu, C.C., Lu, M.C., Wang, W.Y. & Lu, Y.Y., Distance measurement based on pixel variation of CCD images. *ISA Transactions*, **48**(4), pp. 389–395, 2009. http://dx.doi.org/10.1016/j.isatra.2009.05.005

[21] Li, G.D., Lu, G. & Yan, Y., Fire detection using stereoscopic imaging and image processing techniques. *Proceeding of International Conferences on Imaging Systems and Techniques*, IEEE Instrument and Measurement Society, Greece, pp. 28–32, 2014. http://dx.doi.org/10.1109/ist.2014.6958440

[22] Verstockt, S., Van, H.S., Tilley, N., Merci, B., Sette, B., Lambert, P., Hollemeersch, C. & Vande, W.R., Fire cube: a multi-view localization framework for 3D fire analysis. *Fire Safety Journal*, **46**(5), pp. 262–275, 2011. http://dx.doi.org/10.1016/j.firesaf.2011.03.001

[23] Lauer, M., Miriam, S., Lange, S. & Welker, S., 3D-objecttracking with a mixed omnidirectional stereo camera system. *Mechatronics*, **21**(2), pp. 390–398, 2011. http://dx.doi.org/10.1016/j.mechatronics.2010.05.007

[24] Xin, Y.B., Sai, T., Jiang, F.H., Yin, R., Yao, B., Zhang, K.N. & Liu, B.H., An experimental study of automatic water cannon systems for fire protection of large open spaces. *Fire Technology*, **50**(2), pp. 233–248, 2014. http://dx.doi.org/10.1007/s10694-013-0363-4

[25] Qiang, L., Estimation of fire detection time. *Procedia Engineering*, **11**, pp. 233–241, 2011. http://dx.doi.org/10.1016/j.proeng.2011.04.652

[26] Foggia, P., Saggese, A. & Vento, M., Real-time fire detection for video surveillance applications using a combination of experts based on color, shape and motion. *IEEE Transactions on Circuits and Systems for Video Technology*, **25**(9), pp. 1545–1556, 2015. http://dx.doi.org/10.1109/TCSVT.2015.2392531

[27] Escarra, M.D., Le, L.T., Urban, N.M., Oppenheimer, M. & Gmachl, C.F., Quantum cascade laser-based sensing for carbon sequestration leakage monitoring. *IEEE Sensors Journal*, **13**(6), pp. 2348–2356, 2013. http://dx.doi.org/10.1109/JSEN.2013.2253731

[28] Zhou, J., Gao, Y.H., Liu, C.Y. & Zhang, Y.C., Attitude calculation of single camera visual system based on adaptive algorithm. *Optics and Precision Engineering*, **20**(12), pp. 2796–2803, 2012. http://dx.doi.org/10.3788/OPE.20122012.2796

[29] Iyogun, C.O., Birouk, M. & Popplewell, N., Trajectory of water jet exposed to low subsonic cross-flow. *Atomization and Sprays*, **16**(8), pp. 963–979, 2006. http://dx.doi.org/10.1615/AtomizSpr.v16.i8.70

[30] Sun, W.L., Research on intelligent fire systems based on computer vision. *Graduate University of Nanjing University of Aeronautics and Astronautics*, Nanjing, 2011.

[31] Xuan Truong, T. & Kim, Jong-M., Fire flame detection in video sequences using multistage pattern recognition techniques. *Engineering Applications of Artificial Intelligence*, **25**(7), pp. 1365–1372, 2012. http://dx.doi.org/10.1016/j.engappai.2012.05.007

[32] Zhao, H.W., Chen, X., Liu, P.P. & Geng, Q.T., Adaptive segmentation for visual salient object. *Optics and Precision Engineering*, **21**(2), pp. 531–538, 2013. http://dx.doi.org/10.3788/OPE.20132102.0531